ACS Macro Letters

Letter

pubs.acs.org/macroletters

Single Step Process for Self-Assembled Block Copolymer Patterns via in Situ Annealing during Spin-Casting

Hyunjung Jung,[†] Sanghoon Woo,[†] Youngson Choe,[‡] Du Yeol Ryu,[§] June Huh,*[,†] and Joona Bang*[,†]

[†]Department of Chemical and Biological Engineering, Korea University, Seoul 136-713, Republic of Korea

[‡]Department of Chemical Engineering, Pusan National University, Kumjeong-ku, Busan 609-735, Republic of Korea

[§]Department of Chemical and Biolomolecular Engineering, Yonsei University, Seoul 120-749, Republic of Korea

S *Supporting Information*

ABSTRACT: We demonstrated a simple and time-efficient processing method for facilitating a microphase separation of block copolymers (BCPs) based on a single step of spin-casting with low volatile solvent and in situ annealing. Well-ordered lamellar patterns of poly(styrene-*b*-methyl methacrylate) BCP films having wide range of molecular weights (51–235 kg/mol) were fabricated by a single 3 min process of spin-casting, even without the conventional pretreatment of substrate neutralization. The formation of this well-ordered lamellar structure is attributed to a synergetic effect between slow solvent evaporation and thermal energy that may provide an efficient cooling profile for the BCP film during the spin-casting process.

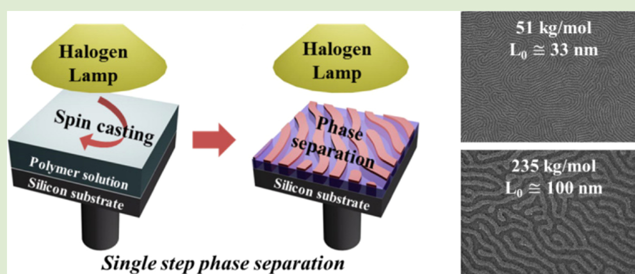

Patterning via self-assembly of block copolymers (BCPs) can be regarded as one of the promising alternatives that overcome the technological and economical limitations associated with photolithographic approaches.[1−6] For instance, with a number of advantages intrinsic to polymer materials, this cost-effective patterning method is expected to replace in part conventional lithographic process for nanoelectronics applications.[7−11] However, despite this potential usability, many technological issues regarding the pattern fidelity and high throughput still remain unresolved, bottlenecking the viability of BCP patterning technology to be used in the actual applications.

Low throughput, which is basically due to the slow ordering kinetics of BCPs in molten state, is one of the main obstacles preventing the practical commercialization for BCP patterning. The most common and traditional process for the pattern formation of BCPs relies on the sequential process consisting of substrate neutralization, spin-casting, and thermal annealing (TA), which undesirably takes several hours or days for achieving sufficient phase separation.[12−18] Many works have been done to facilitate the ordering kinetics of BCP thin film, which commonly employs the solvent vapor annealing (SVA) method to infiltrate solvent vapor into the BCP film in the course of phase-separation.[11,19−21] These works have demonstrated that BCPs under SVA become phase-separated more rapidly with enhanced order than under TA, possibly due to lowered local free energy barriers on the ordering pathway as well as the drastic increase in chain mobility in the solvent-swollen film. In particular, recent SVA approaches suggested that the ordering kinetics is even more facilitated when additional stimuli are combined with SVA.[22−26] Buriak and co-workers demonstrated the ultrafast formation of the BCP pattern using microwaves that instantaneously elevated the solvent vapor pressure and the annealing temperature accelerating ordering kinetics.[25] Ross and co-workers employed a solvothermal annealing setup combining TA and SVA for BCP film accomplishing excellent order within few minutes,[23] which indicates a synergetic effect on facilitating BCP ordering kinetics. While these combined approaches based on SVA is certainly promising for high-throughput BCP patterning in a sense that the annealing process can be completed within a few minutes, the complexity associated with the annealing setup needs to be further refined for the practical use. In this context, a simple and fast patterning method without loss of pattern quality would be highly desirable. Here, we report a highly efficient method for fabricating patterned BCP film that can be completed in 3–4 min only by a single step process of spin-casting. The proposed method therefore does not necessitate the further annealing process as well as the substrate neutralization, minimizing the BCP patterning process without loss of pattern quality.

Our method is based on the spin-casting of BCP solution drop with the use of low volatile solvent while thermal annealing in situ. Scheme 1 depicts the experimental setup for our method. The in situ annealing during spin-casting is designed simply by a halogen lamp (100 W PAR 30 Flood) on top of the spin coating chuck. The distance between the halogen lamp and the coating sample were kept constant at 10

Received: March 27, 2015
Accepted: June 1, 2015
Published: June 3, 2015

 © 2015 American Chemical Society

DOI: 10.1021/acsmacrolett.5b00214
ACS Macro Lett. 2015, 4, 656−660

Scheme 1. Schematic Illustration of Spin-Casting Subjected to In Situ Annealing

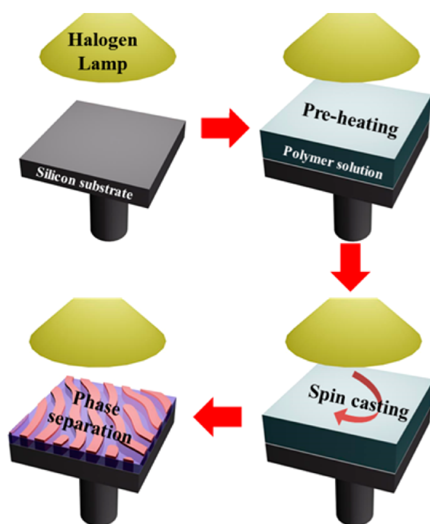

cm during the spin-casting while the luminous intensity from halogen lamp was adjusted to control the target annealing temperature (see Figure S1 and the detailed information on the heating setup in the Supporting Information). For BCPs, we used lamella-forming symmetric poly(styrene-*b*-methyl methacrylate) (PS-*b*-PMMA) having various molecular weights (M_n = 51, 75, 129, and 235 kg/mol with $Đ$ < 1.1, where M_n is the number-averaged molecular weight and $Đ$ is the dispersity.) The silicon wafer (Si) substrate for spin-casting of BCP was cleaned with DI water, methanol, and acetone under sonication for 15 min. Without substrate neutralization, the silicon wafer interacts preferentially with PMMA block, as confirmed by Si/PMMA and Si/PS interfacial tensions estimated from the contact angles of water and diiodomethane on the silicon wafer using the Young−Owens−Wendt equation (Supporting Information, Table S1).[27] The BCP solution drop on silicon wafer held on the coating chuck was preheated at a stationary state for 30 s to warm up the drop, and then spin-coated under the radiation of heat from halogen lamp for 3 min at 3000 rpm. The thicknesses of the BCP films were controlled by the concentration of BCP solution to be 0.5−1.5 L_0, where L_0 is the interlamellar spacing in bulk state. The L_0s of 51, 75, 129, and 235 kg/mol PS-*b*-PMMA correspond to 28, 41, 66, and 102 nm, respectively. Morphological images were obtained using scanning electron microscopy (SEM) after the reactive ion etching.

The choice of solvent for BCP solution is of prime importance in this method, which should consider two essential prerequisites: (1) solvent should be neutrally good for both PS and PMMA block; (2) solvent should have low volatility so as to have high residence time in the BCP film at the annealing temperature. To investigate the effect of solvent having different volatility, we tested the spin-casting process using four different solvents, toluene, dimethylformamide (DMF), diphenyl ether (DPE), and dibenzyl ether (DBE) for preparation of PS-*b*-PMMA solution. Table 1 summarizes boiling points and Hansen solubility parameters[28] having dispersion (δ_d), polar (δ_p), and hydrogen bonding (δ_h) contributions of the four solvents. The boiling point, which can be a measure for the tendency of nonvolatility of solvent, is in order of DBE, DPE, DMF, and toluene. We also estimated

Table 1. Characteristics of Solvents Used for the Spin Casting Process

	boiling point (°C)	solubility parameter, [δ_d, δ_p, δ_h] (MPa$^{1/2}$)
toluene	110	[18.0, 1.4, 2.0][a]
DMF	153	[17.4, 13.7, 11.3][a]
DPE	258	[19.5, 3.5, 5.8][b]
DBE	298	[17.4, 3.7, 7.4][a]

[a]Ref 29. [b]Ref 28.

the solvent quality of the four solvents for PS and PMMA estimated by the relative energy difference (RED) by[28]

$$\text{RED} = R_o^{-1} [4(\delta_{d,1} - \delta_{d,2})^2 + (\delta_{p,1} - \delta_{p,2})^2 + (\delta_{h,1} - \delta_{h,2})^2]^{1/2} \quad (1)$$

where $\delta_{d,\alpha}$, $\delta_{p,\alpha}$, and $\delta_{h,\alpha}$ are the dispersion, polar, and hydrogen contribution of species α (α = 1 for solvent, α = 2 for polymer), respectively, and R_o is termed the interaction radius for solute polymer representing the boundary radius of a sphere centered at [$\delta_{d,2}$, $\delta_{p,2}$, $\delta_{h,2}$] in the space of [δ_d, δ_p, δ_h] (Supporting Information, Table S2). According to the Hansen solubility parameter approach, a good solvent can be described by RED < 1 (conversely, RED > 1 for poor solvent). As seen in Table S2, the solvents used in this study are good for PS and PMMA except rather amphibolic cases for toluene (good or marginal for PMMA) and DMF (marginal for PS).[28−31] In practice, both BCP solutions in toluene and in DMF were also transparent and did not show any visible sign of phase separation.

Figure 1 shows the SEM images of PS-*b*-PMMA films (M_n = 75 kg/mol) prepared by spin-casting of BCP/toluene for 3 min

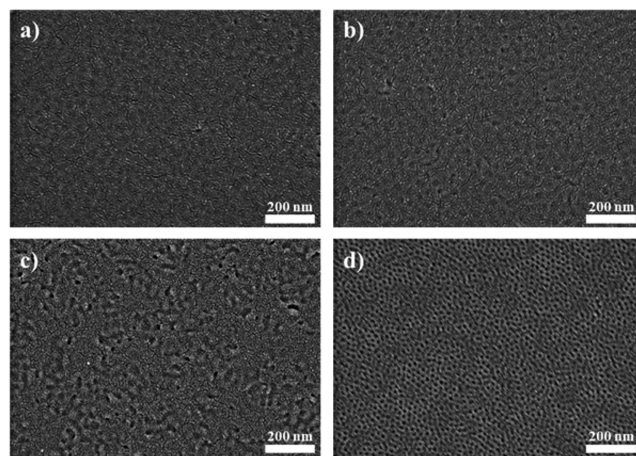

Figure 1. SEM images of symmetric 75 kg/mol PS-*b*-PMMA film prepared by spin-casting for 3 min using toluene as a solvent (a) at 20 °C and (b) at 70 °C, using DMF as a solvent (c) at 20 °C and (d) at 70 °C. For all spin-casted samples, the film thicknesses were adjusted to ∼1.0 L_0.

under in situ annealing at 20 °C (Figure 1a) and 70 °C (Figure 1b), and BCP/DMF for 3 min under in situ annealing at 20 °C (Figure 1c) and 70 °C (Figure 1d), respectively. The poorly ordered micelle-like morphologies in Figure 1a−d reveal that the polymer mobility at this spin-casting condition is not sufficient for the formation of phase separated morphology. In these cases, the rapid evaporation of solvent vitrifies the PS-*b*-PMMA film that has a glass transition temperature (∼100 °C)

DOI: 10.1021/acsmacrolett.5b00214
ACS Macro Lett. 2015, 4, 656−660

higher than the annealing temperature. As for spin-casting using DPE and DBE, the BCP films are not fully dried even after 10 min of spin-casting due to the very low vapor pressure at these temperatures.

By contrast, when the BCP solution with low volatile solvent was spin-casted under an elevated annealing condition, significant morphological changes were observed. Figure 2a,b shows the morphologies of PS-*b*-PMMA film (M_n = 75 kg/mol) prepared by spin-casting of BCP/DPE and BCP/DBE for 3 min under in situ annealing at 200 °C. In the case of the spin-casting of BCP/DPE, the SEM image shows the worm-like domains with many dots, which may be indicative of the lamellar formation in the early stage of assembly. Most notably, the BCP film prepared from BCP/DBE exhibited a well-ordered lamellar morphology with some grains extended over ~1 μm. The well-ordered lamellar structure in this case was also confirmed by grazing-incidence small-angle X-ray scattering (GISAXS) where high order reflections for lamellar structure were clearly seen (Figure 2c, also see the two-dimensional GISAXS pattern in the Supporting Information, Figure S2). We infer that the formation of this well-ordered lamellar structure is attributed to a synergetic effect between slow solvent evaporation and thermal energy that may provide an efficient cooling profile for the BCP film during the spin-casting process. It is worth pointing out that solvent evaporation gives an effect similar to lowering temperature but with much wider range of control for the diffusivity and the (effective) interaction parameters between incompatible blocks (screening interaction by solvent). In order to characterize this cooling effect, we estimated the profile of solvent fraction in the BCP drop, $\phi(t)$, at processing time t as well as the temperature profile, $T(t)$. The profile of solvent fraction was estimated from the measurement of film thickness using the relation $\Delta_\infty/\Delta(t) = 1 - \phi(t)$, where $\Delta(t)$ and Δ_∞ are the thicknesses measured by ellipsometry (SE MG-1000, Nanoview Co.) at time t and after the film is fully dried, respectively. The thickness at a specific time t was measured immediately after stopping spinning at time t. As for $T(t)$, we measured it by a thermocouple probe directly onto the center of samples where angular momentum is null during spin-casting.

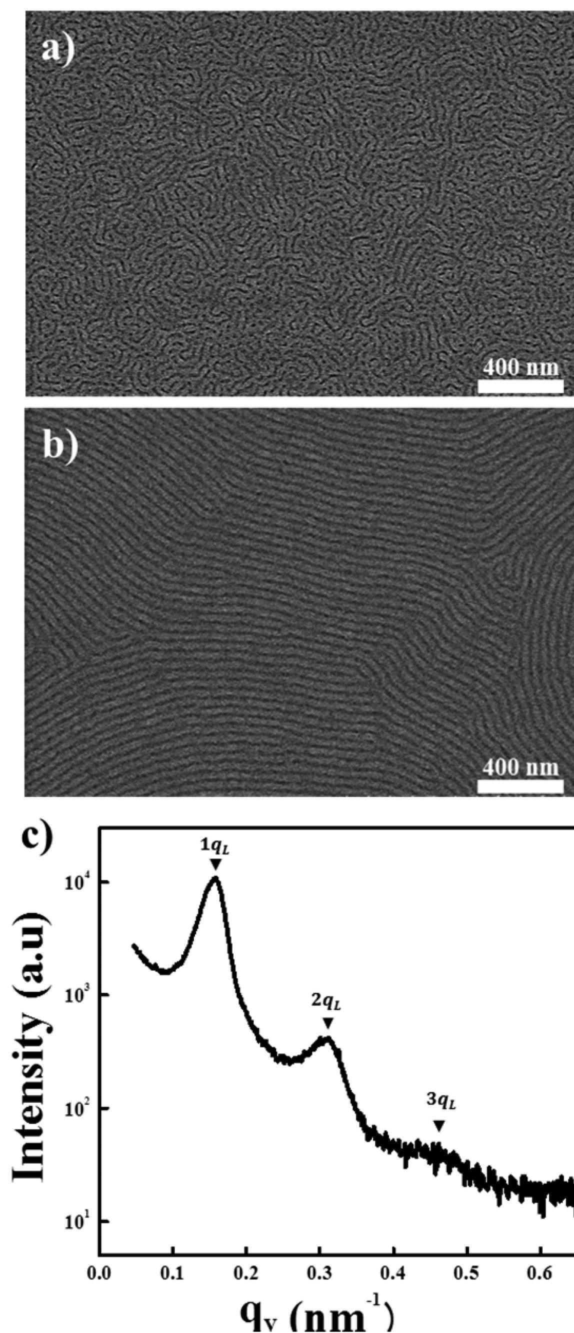

Figure 2. SEM images of symmetric 75 kg/mol PS-*b*-PMMA film prepared by spin-casting for 3 min with in situ annealing at 200 °C using (a) diphenyl ether and (b) dibenzyl ether as a solvent. (c) GISAXS intensity profile of the sample in (b). For all spin-casted samples, the film thicknesses were adjusted to ~1.0 L_0.

Figure 3a shows the variation of the solvent fraction ϕ (solid line) and temperature (dashed line) plotted against time during the processing time span of 0−210 s for the spin-casting system of BCP/DBE under in situ annealing at 200 °C, where the preheating and spin-casting span are indicated by dark and light shaded regions, respectively. The profiles, $\phi(t)$ and $T(t)$, reveal that the solvent content decreases from $\phi \cong 0.93$ (t = 70 s) to $\phi \cong 0.0$ (t > 190 s) with a curve shape similar to a sigmoidal curve, while the temperature remains constant during the nearly entire time span for spin-casting. The solvent fraction at t = 30−70 s could not be measured due to the difficulty in resolving interference oscillations of BCP films from ellipsometry at the early stage of spin-casting process. Based on the characterization of $\phi(t)$ and $T(t)$, we can also estimate the variation of the degree of incompatibility of BCP during the spin-casting, $N\chi_{\text{eff}}(t) = N\chi(T(t))(1 - \phi(t))$, where N is the number of segments per PS-*b*-PMMA BCP chain and the functional $\chi(T(t))$ is the PS−PMMA interaction parameter at $T(t)$ in the absence of solvent.[32,33] As shown in the $N\chi_{\text{eff}}(t)$ profile (Figure 3b), the degree of incompatibility $N\chi_{\text{eff}}(t)$ gradually increases from $N\chi_{\text{eff}} \cong 2$ to $N\chi_{\text{eff}} = 28$ during spin-casting. Therefore, the use of DBE (bp = 298 °C) with in situ annealing at target temperature 200 °C provides the spin-casting process with an effective cooling profile where the initial (effective) temperature, corresponding to $N\chi_{\text{eff}} \cong 2$, is gradually lowered to the target annealing temperature (200 °C) corresponding to $N\chi_{\text{eff}} = 28$. It is well-known from some previous computational works[34−40] that an optimally chosen cooling profile is more efficient for achieving well-equilibrated structure than the isothermal annealing.

We also performed a systematic investigation to find an optimal processing condition by constructing a morphology map covering the variable space of solvent-temperature, which allows us to investigate the isolated effect of one of variables

DOI: 10.1021/acsmacrolett.5b00214
ACS Macro Lett. 2015, 4, 656−660

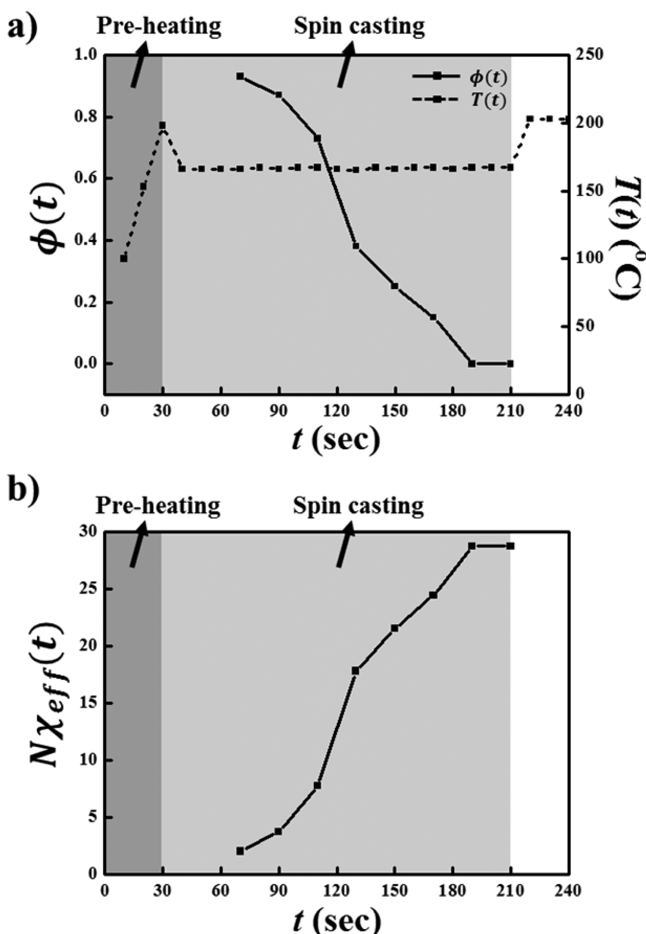

Figure 3. Effective cooling profiles estimated for the spin-casting system of 75 kg/mol PS-*b*-PMMA/DBE under in situ annealing at 200 °C: (a) The solvent fraction in the BCP drop $\phi(t)$ and the temperature $T(t)$ at processing time t; b) the degree of incompatibility $N\chi_{\text{eff}}(t)$ of BCP at processing time t.

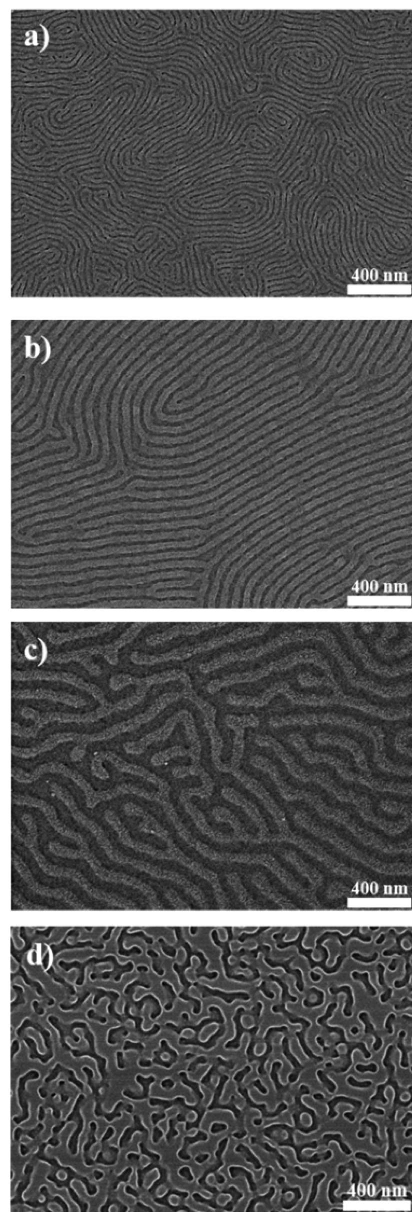

Figure 4. SEM images of symmetric PS-*b*-PMMA films with (a) M_n = 51 kg/mol, (b) 129 kg/mol, (c) 235 kg/mol prepared by spin-casting for 3 min with in situ annealing at 200 °C using dibenzyl ether as a solvent, and (d) 235 kg/mol for 3 days of thermal annealing at 200 °C. The film thicknesses are (a) 32, (b) 65, (c) 98, and (d) 100 nm, which correspond to ~1.0 L_0.

while keeping the other variable constant. For each case, the samples were measured at least three times to ensure the reproducibility of our method. As shown in the morphology map in the variable space of solvent (toluene, DMF, DPE, DBE)-temperature (20, 70, 100, 150, and 200 °C; Supporting Information, Figure S3), elevating temperature gives nearly no effect on the morphological development when high-volatile solvents are used, as seen in the images for toluene and DMF that show only disordered morphologies irrespective of annealing temperature. The morphological changes by varying annealing temperature are only observed for BCP/DPE or BCP/DBE spin-casting systems. In this low-volatile solvent case, the complete removal of solvent from BCP drop is achieved only at high temperatures (>100 °C for DPE and >150 °C for DBE). Well-ordered lamellar structure is obtained for BCP/DBE spin-casting system at 200 °C where the evaporation rate becomes optimal for the morphology development.

This simple procedure of the spin-casting under in situ annealing was also successfully demonstrated for various molecular weight of PS-*b*-PMMA BCPs. Figure 4a−c present the SEM images of PS-*b*-PMMA films with M_n = 51, 129, and 235 kg/mol prepared by the same spin-casting method (spin-casting of BCP/DBE for 3 min while annealing in situ at 200 °C). Well-developed stripe patterns, indicative of the lamellar formation perpendicular to the substrate, are clearly seen even in the spin-casted film. When the films were prepared with different thicknesses (~0.5 L_0 and ~1.5 L_0), it was also observed that they exhibited the well-ordered lamellar structures, suggesting that this process is not sensitive to the film thickness (Supporting Information, Figures S4 and S5). In particular, the lamellar development for BCP with M_n = 235 kg/mol ($L_0 \cong$ 100 nm) by this 3 min process of spin-casting is remarkable when compared to the poorly ordered structures obtained by 3 days of thermal annealing at 200 °C (Figure 4d). It is also worth noting that the films did not exhibit any dewetting or thickness variation that often occur in the post solvent annealing process, because our process is simply based on the spin-casting of BCP solution under elevated temperature

DOI: 10.1021/acsmacrolett.5b00214
ACS Macro Lett. 2015, 4, 656−660

without any post annealing step (Supporting Information, Figure S6).

In summary, we demonstrated a simple and time-efficient BCP patterning method that uses spin-casting of BCP solution with low volatile solvent while annealing in situ. Well-ordered lamellar patterns of PS-*b*-PMMA films having various molecular weights were fabricated by a single 3 min process of spin-casting, which therefore does not require additional pretreatment and postprocess used in the conventional method. The proposed spin-casting method is in many ways advantageous for applying high-throughput production of patterned PS-*b*-PMMA film having wide range of molecular weights, even for highly viscous BCPs (M_n > 200 kg/mol). Furthermore, we believe that this process can be also applicable to other BCP systems with judicious choice of solvent (i.e., solubility and volatility) and casting conditions (i.e., casting time and temperature).

■ ASSOCIATED CONTENT

Supporting Information

Experimental methods and additional GISAXS, SEM, and optical microscopy images. The Supporting Information is available free of charge on the ACS Publications website at DOI: 10.1021/acsmacrolett.5b00214.

■ AUTHOR INFORMATION

Corresponding Authors

*E-mail: junehuh@korea.ac.kr.

*E-mail: joona@korea.ac.kr.

Notes

The authors declare no competing financial interest.

■ ACKNOWLEDGMENTS

This work was by National Research Foundation of Korea grants funded by the Korea government (MSIP; Nos. 2012M3A7B4049863, 2012M3A7B4035323, and NRF-2013R1A1A2064112) and also by the Global Frontier R&D Program (No. 2013M3A6B1078869) on Center for Hybrid Interface Materials (HIM) funded by the Ministry of Science, ICT and Future Planning.

■ REFERENCES

(1) Baghgar, M.; Barnes, A. M.; Pentzer, E.; Wise, A. J.; Hammer, B. A. G.; Emrick, T.; Dinsmore, A. D.; Barnes, M. D. *ACS Nano* **2014**, *8*, 8344−8349.

(2) Black, C. T. *ACS Nano* **2007**, *1*, 147−150.

(3) Bang, J.; Jeong, U.; Ryu, D. Y.; Russell, T. P.; Hawker, C. J. *Adv. Mater.* **2009**, *21*, 4769−4792.

(4) Hawker, C. J.; Russell, T. P. *MRS Bull.* **2005**, *30*, 952−966.

(5) Black, C. T. *Nat. Nanotechnol.* **2007**, *2*, 464−465.

(6) Segalman, R. A. *Mater. Sci. Eng. R* **2005**, *48*, 191−226.

(7) Black, C. T.; Ruiz, R.; Breyta, G.; Cheng, J. Y.; Colburn, M. E.; Guarini, K. W.; Kim, H.-C.; Zhang, Y. *IBM J. Res. Dev.* **2007**, *51*, 605−633.

(8) Thurn-Albrecht, T.; Schotter, J.; Kästle, G. A.; Emley, N.; Shibauchi, T.; Krusin-Elbaum, L.; Guarini, K.; Black, C.; Tuominen, M. T.; Russell, T. P. *Science* **2000**, *290*, 2126−2129.

(9) Khullar, P.; Singh, V.; Mahal, A.; Kumar, H.; Kaur, G.; Bakshi, M. S. *J. Phys. Chem. B* **2013**, *117*, 3028−3039.

(10) Herr, D. J. *J. Mater. Res.* **2011**, *26*, 122−139.

(11) Park, S.; Lee, D. H.; Xu, J.; Kim, B.; Hong, S. W.; Jeong, U.; Xu, T.; Russell, T. P. *Science* **2009**, *323*, 1030−1033.

(12) Mansky, P.; Russell, T. P.; Hawker, C. J.; Pitsikalis, M.; Mays, J. *Macromolecules* **1997**, *30*, 6810−6813.

(13) Bang, J.; Bae, J.; Löwenhielm, P.; Spiessberger, C.; Given-Beck, S. A.; Russell, T. P.; Hawker, C. J. *Adv. Mater.* **2007**, *19*, 4552−4557.

(14) Thurn-Albrecht, T.; Steiner, R.; DeRouchey, J.; Stafford, C. M.; Huang, E.; Bal, M.; Tuominen, M.; Hawker, C. J.; Russell, T. P. *Adv. Mater.* **2000**, *12*, 787−791.

(15) Guarini, K. W.; Black, C. T.; Yeung, S. H. I. *Adv. Mater.* **2002**, *14*, 1290−1294.

(16) Kim, S. O.; Solak, H. H.; Stoykovich, M. P.; Ferrier, N. J.; de Pablo, J. J.; Nealey, P. F. *Nature* **2003**, *424*, 411−414.

(17) Welander, A. M.; Kang, H.; Stuen, K. O.; Solak, H. H.; Müller, M.; de Pablo, J. J.; Nealey, P. F. *Macromolecules* **2008**, *41*, 2759−2761.

(18) Mansky, P.; Liu, Y.; Huang, E.; Russell, T. P.; Hawker, C. J. *Science* **1997**, *275*, 1458−1460.

(19) Kim, S. H.; Misner, M. J.; Xu, T.; Kimura, M.; Russell, T. P. *Adv. Mater.* **2004**, *16*, 226−231.

(20) Jung, Y. S.; Ross, C. A. *Adv. Mater.* **2009**, *21*, 2540−2545.

(21) Thompson, R. L.; McDonald, M. T.; Lenthall, J. T.; Hutchings, L. R. *Macromolecules* **2005**, *38*, 4339−4344.

(22) Park, W. I.; Kim, K.; Jang, H.-I.; Jeong, J. W.; Kim, J. M.; Choi, J.; Park, J. H.; Jung, Y. S. *Small* **2012**, *8*, 3762−3768.

(23) Gotrik, K. W.; Ross, C. *Nano Lett.* **2013**, *13*, 5117−5122.

(24) Borah, D.; Senthamaraikannan, R.; Rasappa, S.; Kosmala, B.; Holmes, J. D.; Morris, M. A. *ACS Nano* **2013**, *7*, 6583−6596.

(25) Zhang, X.; Harris, K. D.; Wu, N. L. Y.; Murphy, J. N.; Buriak, J. M. *ACS Nano* **2010**, *4*, 7021−7029.

(26) Higuchi, T.; Shimomura, M.; Yabu, H. *Macromolecules* **2013**, *46*, 4064−4068.

(27) Owens, D. K.; Wendt, R. C. *J. Appl. Polym. Sci.* **1969**, *13*, 1741−1747.

(28) Hansen, C. M. In *Hansen Solubility Parameters: A User's Handbook*, 2nd ed.; CRC Press: Boca Raton, FL, 2007; pp 335, 408, 495, 498.

(29) Barton, A. F. *CRC Handbook of Solubility Parameters and Other Cohesion Parameters*, 2nd ed.; CRC Press: Boca Raton, FL, 1991; pp 153−157 and 424.

(30) Peng, P.; Shi, B.; Jia, L.; Li, B. *J. Macromol. Sci., Part B: Phys.* **2010**, *49*, 864−869.

(31) van Dyk, J. W.; Frisch, H. L.; Wu, D. T. *Ind. Eng. Chem. Prod. Res. Dev.* **1985**, *24*, 473−478.

(32) Zhao, Y.; Sivaniah, E.; Hashimoto, T. *Macromolecules* **2008**, *41*, 9948−9951.

(33) Russell, T. P.; Hjelm, R. P., Jr; Seeger, P. A. *Macromolecules* **1990**, *23*, 890−893.

(34) Chakrabarti, A.; Gunton, J. D. *Phys. Rev. E* **1993**, *47*, R792.

(35) Sun, P.; Yin, Y.; Li, B.; Chen, T.; Jin, Q.; Ding, D.; Shi, A.-C. *J. Chem. Phys.* **2005**, *122*, 204905.

(36) Yu, B.; Li, B.; Sun, P.; Chen, T.; Jin, Q.; Ding, D.; Shi, A.-C. *J. Chem. Phys.* **2005**, *123*, 234902.

(37) Pinna, M.; Zvelindovsky, A. *Eur. Phys. J. B* **2012**, *85*, 1−18.

(38) Hajek, B. *Math. Oper. Res.* **1988**, *13*, 311−329.

(39) Chakrabarti, A.; Toral, R. *Phys. Rev. B* **1989**, *39*, 542−545.

(40) Grest, G. S.; Soukoulis, C.; Levin, K. *Phys. Rev. Lett.* **1986**, *56*, 1148−1151.